

# High-Sensitivity Ion Mobility Spectrometry/Mass Spectrometry Using Electrodynamic Ion Funnel Interfaces

Keqi Tang, Alexandre A. Shvartsburg, Hak-No Lee, David C. Prior, Michael A. Buschbach, Fumin Li, Aleksey V. Tolmachev, Gordon A. Anderson, and Richard D. Smith\*

Biological Sciences Division and Environmental Molecular Sciences Laboratory, Pacific Northwest National Laboratory, P.O. Box 999, Richland, Washington 99352

The utility of ion mobility spectrometry (IMS) for separation of mixtures and structural characterization of ions has been demonstrated extensively, including in biological and nanoscience contexts. A major attraction of IMS is its speed, several orders of magnitude greater than that of condensed-phase separations. Nonetheless, IMS combined with mass spectrometry (MS) has remained a niche technique, substantially because of limited sensitivity resulting from ion losses at the IMS-MS junction. We have developed a new electrospray ionization (ESI)-IMS-QTOF MS instrument that incorporates electrodynamic ion funnels at both front ESI-IMS and rear IMS-QTOF interfaces. The front funnel is of the novel “hourglass” design that efficiently accumulates ions and pulses them into the IMS drift tube. Even for drift tubes of 2-m length, ion transmission through IMS and on to QTOF is essentially lossless across the range of ion masses relevant to most applications. The rf ion focusing at the IMS terminus does not degrade IMS resolving power, which exceeds 100 (for singly charged ions) and is close to the theoretical limit. The overall sensitivity of the present ESI-IMS-MS system is comparable to that of commercial ESI-MS, which should make IMS-MS suitable for analyses of complex mixtures with ultrahigh sensitivity and exceptional throughput.

Ion mobility spectrometry (IMS) had been known since 1970s as a tool for analysis and characterization of gas-phase ions.<sup>1–5</sup> In particular, IMS has been used to separate mixtures<sup>6–9</sup> (including isomeric mixtures<sup>8,9</sup>), detect and quantify the presence of specific

analytes,<sup>10–12</sup> and characterize the molecular structure of novel chemical species.<sup>2,4,13–20</sup>

IMS exploits the fact that different particles diffuse through a gas at different speeds, depending on their collision cross sections with the gas molecules. While neutrals diffuse by random Brownian motion, ions in an electric field drift in a defined direction with the velocity controlled by their mobility ( $K$ ). This quantity varies with the field intensity  $E$  in general, but IMS is typically run in a low-field regime where  $K(E)$  is nearly constant. In that limit,  $K$  depends on the ion/buffer gas cross section<sup>21,22</sup> (rigorously the first-order orientationally averaged collision integral  $\Omega_{av}^{(1,1)}$ ). This allows a spatial separation of different ions, including structural isomers.

At the simplest, an IMS instrument consists of a tube filled with a nonreactive buffer gas (commonly He or N<sub>2</sub>), a generally uniform electric field established along the axis, and a charge/ion detector at the end. Separated species are characterized by their different mobilities, derived from the measured drift times by adjusting for  $E$ , gas number density  $N$ , and tube length  $L$ . The technology has been widely deployed to monitor the environmental air and water, track industrial processes and ensure product quality, and detect explosives or chemical warfare agents in

\* Corresponding author. Tel.: (509) 376-0732. Fax: (509) 376-2303.

- (1) Hill H. H.; Siems, W. F.; St. Louis, R. H.; McMinn, D. G. *Anal. Chem.* **1990**, *62*, A1201.
- (2) Bowers, M. T.; Kemper, P. R.; von Helden, G.; van Koppen, P. A. M. *Science* **1993**, *260*, 1446.
- (3) Shvartsburg, A. A.; Hudgins, R. R.; Dugourd, P.; Jarrold, M. F. *Chem. Soc. Rev.* **2001**, *30*, 26.
- (4) Hoaglund-Hyzer, C. S.; Lee, Y. J.; Counterman, A. E.; Clemmer, D. E. *Anal. Chem.* **2002**, *74*, 992.
- (5) Collins, D. C.; Lee, M. L. *Anal. Bioanal. Chem.* **2002**, *372*, 66.
- (6) Barnes, C. A. S.; Hilderbrand, A. E.; Valentine, S. J.; Clemmer, D. E. *Anal. Chem.* **2002**, *74*, 26.
- (7) Moon, M. H.; Myung, S.; Plascencia, M.; Hilderbrand, A. E.; Clemmer, D. E. *J. Proteome Res.* **2003**, *2*, 589.
- (8) Wu, C.; Siems, W. F.; Klasmeier, J.; Hill, H. H. *Anal. Chem.* **2000**, *72*, 391.

- (9) Fromherz, R.; Gantefor, G.; Shvartsburg, A. A. *Phys. Rev. Lett.* **2002**, *89*, No. 083001.
- (10) Beegle, L. W.; Kanik, I.; Matz, L.; Hill, H. H. *Anal. Chem.* **2001**, *73*, 3028.
- (11) Srebalus, C. A.; Li, J. W.; Marshall, W. S.; Clemmer, D. E. *J. Am. Soc. Mass Spectrom.* **2000**, *11*, 352.
- (12) Counterman, A. E.; Clemmer, D. E. *Anal. Chem.* **2002**, *74*, 1946.
- (13) Lee, S. H.; Gotts, N. G.; von Helden, G.; Bowers, M. T. *Science* **1995**, *267*, 999.
- (14) Wytenbach, T.; Bushnell, J. E.; Bowers, M. T. *J. Am. Chem. Soc.* **1998**, *120*, 5098.
- (15) Wytenbach, T.; Bowers, M. T. *Top. Curr. Chem.* **2003**, *225*, 207.
- (16) Shvartsburg, A. A.; Hudgins, R. R.; Gutierrez, R.; Jungnickel, G.; Frauenheim, T.; Jackson, K. A.; Jarrold, M. F. *J. Phys. Chem. A* **1999**, *103*, 5275.
- (17) Shvartsburg, A. A.; Hudgins, R. R.; Dugourd, P.; Gutierrez, R.; Frauenheim, T.; Jarrold, M. F. *Phys. Rev. Lett.* **2000**, *84*, 2421.
- (18) Jackson, K. A.; Horoi, M.; Chaudhuri, I.; Frauenheim, T.; Shvartsburg, A. A. *Phys. Rev. Lett.* **2004**, *93*, No. 013401.
- (19) Leavell, M. D.; Gaucher, S. P.; Leary, J. A.; Taraszka, J. A.; Clemmer, D. E. *J. Am. Soc. Mass Spectrom.* **2002**, *13*, 284.
- (20) Myung, S.; Badman, E. R.; Lee, Y. J.; Clemmer, D. E. *J. Phys. Chem. A* **2002**, *106*, 9976.
- (21) Mason, E. A.; McDaniel, E. W. *Transport Properties of Ions in Gases*; Wiley: New York, 1988.
- (22) Mesleh, M. F.; Hunter, J. M.; Shvartsburg, A. A.; Schatz, G. C.; Jarrold, M. F. *J. Phys. Chem.* **1996**, *100*, 16082.

security and defense applications.<sup>1,23–27</sup> However, until the 1990s IMS was primarily perceived as a relatively inexpensive, low-power, compact alternative to mass spectrometry (MS) suitable for field analyses.

The interest in coupling IMS to MS has been increasing over the past decade. It was first implemented using quadrupole MS,<sup>28,29</sup> which necessitated either measuring separate IMS spectra for each  $m/z$  value of interest or, alternatively, scanning the  $m/z$  for each peak of interest selected from the IMS spectrum and necessarily repeated over many IMS separations. However, real-world bioanalytical applications were limited because of low throughput and insufficient sensitivity. This situation changed with the coupling of IMS to time-of-flight (TOF) MS.<sup>30–34</sup> The IMS-TOF combination permits a concurrent dispersion of mixture components in two dimensions: ion mobility and  $m/z$ . Since an IMS separation typically requires  $\sim 1$ – $100$  ms and has the resolving power of  $10$ – $200$ , a single species in an IMS ion packet (i.e., peak) often appears over a  $\sim 0.1$ – $1$ -ms period. A typical TOF cycle is  $\sim 10$ – $100$   $\mu$ s long, so one or more mass spectra can be obtained during the “elution” of an IMS peak. This enables the 2-D analysis of an ion mixture with potentially perfect ion utilization efficiency. An IMS-MS system may be enhanced to address greater levels of sample complexity by addition of an upstream condensed-phase separation such as liquid chromatography (LC), creating a 2-D separation followed by MS analysis.<sup>7,33,34</sup> Characteristic time scales of LC and IMS also match well: a single LC peak normally elutes over 5–30 s, allowing for  $\sim 10^2$ – $10^4$  IMS-MS analyses.

IMS can be comparable to condensed-phase separations in resolution, but greatly superior in speed. That is, the resolving power ( $R$ ) of IMS<sup>32,35,36</sup> can exceed 100 (and 200 for multiply charged ions<sup>32,37</sup> that are typical of peptides from tryptic digests). However, an IMS separation requires  $<100$  ms, while current condensed-phase separations require orders of magnitude longer. Thus, IMS may provide the basis for increasing the throughput of analyses, which is generally crucial for real proteomics, metabolomics, and other biological studies involving highly complex samples. For multidimensional separations involving IMS,

for example, an LC run with peak capacity of  $\sim 50$  in 2–3 min<sup>38</sup> can potentially provide a combined LC-IMS separation peak capacity of  $>1000$  on the same time scale. In comparison, a 2-D liquid-phase strong-cation exchange and reversed-phase LC (Mud-PIT)<sup>39,40</sup> separation with peak capacity of  $\sim 3000$  typically requires over 24 h, and 2-D gel electrophoresis<sup>41</sup> with peak capacity of  $10^3$ – $10^4$  requires  $\sim 10$  h.

Despite an enormous potential for high-throughput analyses of complex samples, the application of IMS-MS (and LC-IMS-MS) has been limited by low sensitivity arising primarily from ion losses at the IMS-MS interface. Ion packets traveling through the IMS experience thermal diffusion<sup>42</sup> and (at high ion currents) Coulomb expansion<sup>43</sup> superposed on the directed drift motion, which produces spatial broadening. The component of this broadening along the drift axis is responsible for the finite IMS resolution. The broadening perpendicular to that axis limits the fraction of ions that exit IMS, since the exit aperture is generally much smaller than the size of arriving ion packets. The vacuum needed for the subsequent MS stage and the relatively high pressure required by IMS constrain the practical diameter of the aperture connecting these stages ( $\Theta$ ), which results in large ion losses. To estimate them, we assume an isotropic broadening of ion packets in IMS. (In principle, an electric field renders the broadening anisotropic, preferentially augmenting the component along the drift axis.<sup>44</sup> In the low-field regime typical for IMS, this effect is small.) Then the spherical diameter of ion packet at the IMS end  $W_0$  (the full width at half-maximum, fwhm) equals its width along the drift axis. By the definition of  $R$ ,  $W_0 = L/R$ , and the area of ion impact on the IMS exit is  $\sim (\pi/4)(L/R)^2$ . Since in practical IMS designs  $L/R \gg \Theta$ , the ion transmission efficiency ( $S$ ) through IMS is given by

$$S \sim (\Theta R/L)^2. \quad (1)$$

At low  $E$  and ignoring space-charge effects,  $R$  is ideally<sup>45</sup>

$$R = t_D / [t_p^2 + (t_D/R_d)^2]^{1/2} \quad (2)$$

where  $t_p$  is the (temporal) width of initial packet,  $t_D$  is the drift time, and  $R_d$  is the maximum IMS resolving power limited only by thermal diffusion:

$$R_d = \left( \frac{LEze}{16k_B T \ln 2} \right)^{1/2} \quad (3)$$

where  $ze$  is the ionic charge,  $k_B$  is the Boltzmann constant, and  $T$  is the gas temperature. (Equation 2 is rigorous for initially spherical ion packets only.) In the limit of  $R \Rightarrow R_d$ , eqs 1 and 3 yield

- (23) Eiceman, G. A.; Leasure, C. S.; Vandiver, V. J. *Anal. Chem.* **1986**, *58*, 76.  
 (24) Lawrence, A. H.; Neudorfl, P. *Anal. Chem.* **1988**, *60*, 104.  
 (25) Lopez-Avila, V.; Hill, H. H. *Anal. Chem.* **1997**, *69*, 289R.  
 (26) Przybylko, A. R. M.; Thomas, C. L. P.; Anstice, P. J.; Fielden, P. R.; Brokenshire, J.; Irons, F. *Anal. Chim. Acta* **1995**, *311*, 77.  
 (27) Wu, C.; Siems, W. F.; Hill, H. H.; Hannan, R. M. *J. Chromatogr., A* **1998**, *811*, 157.  
 (28) von Helden, G.; Hsu, M. T.; Kemper, P. R.; Bowers, M. T. *J. Chem. Phys.* **1991**, *95*, 3835.  
 (29) Jarrold, M. F.; Constant, V. A. *Phys. Rev. Lett.* **1991**, *67*, 2994.  
 (30) Guevremont, R.; Siu, K. W. M.; Wang, J. Y.; Ding, L. Y. *Anal. Chem.* **1997**, *69*, 3959.  
 (31) Hoaglund, C. S.; Valentine, S. J.; Sporleder, C. R.; Reilly, J. P.; Clemmer, D. E. *Anal. Chem.* **1998**, *70*, 2236.  
 (32) Srebalus, C. A.; Li, J.; Marshall, W. S.; Clemmer, D. E. *Anal. Chem.* **1999**, *71*, 3918.  
 (33) Lee, Y. J.; Hoaglund-Hyzer, C. S.; Srebalus Barnes, C. A.; Hilderbrand, A. E.; Valentine, S. J.; Clemmer, D. E. *J. Chromatogr., B* **2002**, *782*, 343.  
 (34) Myung, S.; Lee, Y. J.; Moon, M. H.; Taraszka, J.; Sowell, R.; Koeniger, S.; Hilderbrand, A. E.; Valentine, S. J.; Cherbas, L.; Cherbas, P.; Kaufmann, T. C.; Miller, D. F.; Mechref, Y.; Novotny, M. V.; Ewing, M. A.; Sporleder, C. R.; Clemmer, D. E. *Anal. Chem.* **2003**, *75*, 5137.  
 (35) Asbury, G. R.; Hill, H. H. *J. Microcolumn. Sep.* **2000**, *12*, 172.  
 (36) Dugourd, Ph.; Hudgins, R. R.; Clemmer, D. E.; Jarrold, M. F. *Rev. Sci. Instrum.* **1997**, *68*, 1122.  
 (37) Wu, C.; Siems, W. F.; Asbury, G. R.; Hill, H. H. *Anal. Chem.* **1998**, *70*, 4929.

- (38) Issaeva, T.; Kourganov, A.; Unger, K. J. *Chromatogr., A* **1999**, *846*, 13.  
 (39) Washburn, M. P.; Wolters, D.; Yates, J. R. *Nat. Biotechnol.* **2001**, *19*, 242.  
 (40) Wolters, D. A.; Washburn, M. P.; Yates, J. R. *Anal. Chem.* **2001**, *73*, 5683.  
 (41) Gygi, S. P.; Corthals, G. L.; Zhang, Y.; Rochon, Y.; Aebersold, R. *Proc. Natl. Acad. Sci. U.S.A.* **2000**, *97*, 9390.  
 (42) Rokushika, S.; Hatano, H.; Baim, M. A.; Hill, H. H. *Anal. Chem.* **1985**, *57*, 1902.  
 (43) Spangler, G. E. *Anal. Chem.* **1992**, *64*, 1312.  
 (44) Verbeck, G. F.; Ruotolo, B. T.; Gillig, K. J.; Russell, D. H. *J. Am. Soc. Mass Spectrom.* **2004**, *15*, 1320.  
 (45) Siems, W. F.; Wu, C.; Tarver, E. A.; Hill, H. H.; Larsen, P. R.; McMinn, D. G. *Anal. Chem.* **1994**, *66*, 4195.

$$S \sim \left( \frac{\Theta E z e}{16 k_B T R \ln 2} \right)^2 \quad (4)$$

That is, when the injected ion packet is very “thin” compared to the drift time and small compared to the broadening by IMS terminus, IMS-MS sensitivity is inversely proportional to the IMS resolving power squared. This remains approximately true for finite initial packets in realistic IMS designs, where the  $S(R)$  dependence is derived by combining eqs 1 and 2. This circumstance had severely limited the practically achievable IMS resolution and peak capacity.

For instance, an ion packet is  $\sim 5$  mm in diameter at the exit of 76-mm-long drift tube<sup>29</sup> in one MS-IMS-MS design operating at a pressure of  $P$  of  $\sim 5$  Torr (and providing  $R \sim 15$ ). In that instrument,  $\Theta = 0.25$  mm, and according to eq 4,  $< 1\%$  of the ions traversing the IMS are transmitted to the following MS stage. An IMS resolving power of 15 is inadequate for many applications. Higher resolution IMS-MS instruments require drift tubes that are longer (and thus yield broader ion packets), operate at higher gas pressures (which requires even narrower apertures), or both; thus, ion transmission efficiency is even lower. For example, an instrument<sup>36</sup> with  $R \sim 170$  ( $L = 63$  cm and  $\Theta = 0.12$  mm) operated at  $P \sim 500$  Torr would have  $\sim 99.9\%$  of ions lost at the exit aperture. Equation 4 may still underestimate losses, as it ignores the finite initial size of ion packets and additional broadening by Coulomb repulsion, though this is somewhat balanced by (also neglected) gas dynamic effects near the IMS exit aperture that increase its effective diameter. Regardless, ion losses are substantial.

An ideal IMS-MS interface, similar to the electrospray ionization (ESI)-MS interface, should efficiently transmit incoming ions through a narrow aperture that maintains a large pressure differential. In both custom<sup>46</sup> and commercial<sup>47</sup> instruments, ESI and other API sources are commonly coupled to MS analyzers using differentially pumped orifice (or capillary)–skimmer cone (OSC) arrangements. Differential pumping between IMS and MS allows a wider IMS exit aperture and can improve ion transmission. In fact, an OSC design at the IMS terminus<sup>4,33,48–50</sup> has been shown to improve IMS-MS sensitivity<sup>48</sup> by a factor of 5–10. Considering the ion transmission of  $< 1\%$  in earlier designs, this improvement still implies  $> 90\text{--}95\%$  ion loss at the IMS-MS interface. Indeed, Clemmer and co-workers<sup>4</sup> have pointed out that “although improvements in sensitivity have been demonstrated, the current technologies are still not as sensitive as the well-developed MS-MS strategies, however we believe that much of this difference will be diminished as additional improvements in the instruments are made.”

The device of choice for efficiently conveying ions from regions of moderately high pressure ( $\sim 1\text{--}10$  Torr) into vacuum is the electrodynamic ion funnel.<sup>51–53</sup> The ion funnel consists of a stack of insulated electrodes carrying an axial dc gradient and a

harmonic rf potential applied to adjacent electrodes with opposite phases. Each electrode features a circular aperture that narrows along the stack. An ion packet entering the funnel via its widest aperture is pushed through by the dc gradient, while confined radially by the rf field. The entrance aperture may be as large as 5 cm (or greater) to accept diffuse beams. The small exit aperture, generally  $\sim 2$  mm, provides a tight focusing of those beams through a dc-only orifice immediately following the funnel. The exceptional performance of ion funnels in ESI-MS (including quadrupole, TOF, and FTICR) interfaces has been demonstrated extensively,<sup>51–56</sup> allowing, for example, zeptomole sensitivity using ESI-FTICR.<sup>54</sup> In a direct comparison, an ion funnel ESI-MS interface<sup>55</sup> has provided over 1 order of magnitude sensitivity improvement over a conventional OSC design. The gain at the ESI-IMS interface should be comparable, and that at the IMS terminus should be even greater due to a near-absence of gas dynamic disturbances. (In ESI-MS interfaces, the jet exiting the heated capillary expands inside the funnel, creating strong gas flows that can reduce the electrodynamic ion confinement and degrade efficiency.) Most importantly, an ion funnel can transmit close to 100% of incoming analyte ions over a broad  $m/z$  range,<sup>56</sup> which should enable much more sensitive IMS-MS instrumentation.

Here we describe a new ESI-IMS-QTOF instrument incorporating ion funnels at both ESI-IMS and IMS-QTOF interfaces. Despite the drift tube length of 210 cm, the ion transmission through the IMS is near-perfect across a broad  $m/z$  range.

## EXPERIMENTAL SECTION

The ESI-IMS-QTOF instrument (Figure 1) comprises three major components: ESI source, IMS drift tube, and QTOF MS that analyses ion packets separated by IMS. The work reported here has used positive ions produced by ESI, and the voltages on all elements are given accordingly. To analyze anions, all polarities would have to be reversed.

**ESI Source.** The source consists of an ESI emitter followed by a heated capillary inlet (both standard in modern ESI-MS) and a novel “hourglass” ion funnel for pulsed ion transmission described below. The emitter is mounted on an X–Y translation stage allowing fine position adjustment with respect to the inlet. A microsyringe driven by a pump (KD Scientific, Holliston, MA) was used to infuse samples to the ESI emitter through a metal union. The ESI source is electrically floated above the IMS voltage (see below) using adjustable rf and dc power supplies; all voltages stated in this subsection are referenced to the IMS voltage. The union and emitter are at a potential of 2–2.5 kV above the inlet. The ions generated by ESI are sampled into an inlet capillary (0.43 mm i.d. and 64 mm long) heated by two cartridge heaters.<sup>56</sup> The temperature ( $\sim 120$  °C) is monitored by thermocouples and regulated using a closed-loop control unit (Omega CN9000A). The

(46) Smith, R. D.; Loo, J. A.; Edmonds, C. G.; Barinaga, C. J.; Udseth, H. R. *Anal. Chem.* **1990**, *62*, 882.

(47) Sannes-Lowery, K.; Griffey, R. H.; Kruppa, G. H.; Speir, J. P.; Hofstadler, S. A. *Rapid Commun. Mass Spectrom.* **1998**, *12*, 1957.

(48) Lee, Y. J.; Hoaglund-Hyzer, C. S.; Taraszka, J. A.; Zientara, G. A.; Counterman, A. E.; Clemmer, D. E. *Anal. Chem.* **2001**, *73*, 3549.

(49) Valentine, S. J.; Koeniger, S. L.; Clemmer, D. E. *Anal. Chem.* **2003**, *75*, 6202.

(50) Weis, P.; Gilb, S.; Gerhardt, P.; Kappes, M. M. *Int. J. Mass Spectrom.* **2002**, *216*, 59.

(51) Shaffer, S. A.; Tang, K.; Anderson, G. A.; Prior, D. C.; Udseth, H. R.; Smith, R. D. *Anal. Chem.* **1998**, *70*, 4111.

(52) Shaffer, S. A.; Tolmachev, A.; Prior, D. C.; Anderson, G. A.; Udseth, H. R.; Smith, R. D. *Anal. Chem.* **1999**, *71*, 2957.

(53) Smith, R. D.; Shaffer, S. A. U.S. Patent 6,107,628, 2000.

(54) Belov, M. E.; Gorshkov, M. V.; Udseth, H. R.; Anderson, G. A.; Smith, R. D. *Anal. Chem.* **2000**, *72*, 2271.

(55) Kim, T.; Udseth, H. R.; Smith, R. D. *Anal. Chem.* **2000**, *72*, 5014.

(56) Kim, T.; Tolmachev, A. V.; Harkewicz, R.; Prior, D. C.; Anderson, G. A.; Udseth, H. R.; Smith, R. D.; Bailey, T. H.; Rakov, S.; Futrell, J. H. *Anal. Chem.* **2000**, *72*, 2247.

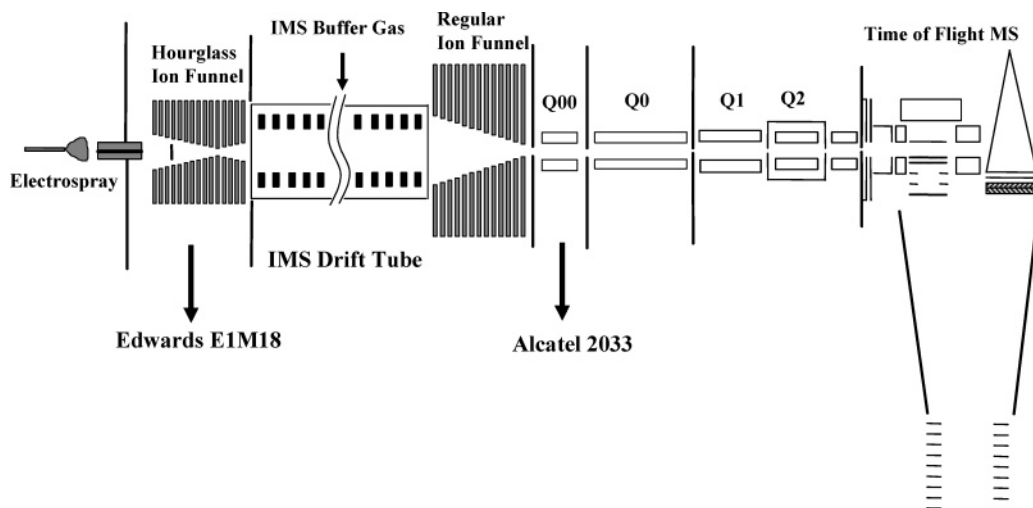


**Figure 1.** Schematic of the ESI-IMS-QTOF instrumentation interfaced using electrodynamic ion funnels.

dc bias on the capillary is 350 V. The ESI emitter voltage and position were adjusted to optimize instrumental sensitivity.

Ions exiting the heated capillary enter the hourglass-shaped ion funnel mounted inside a steel vacuum chamber floated at the voltage of that capillary. The chamber is mechanically pumped (Edwards E1M18, 5.7 L/s) through an insulating hose of reinforced plastic. A flow valve on the hose permits the control of chamber pressure down to  $\sim 1$  Torr. While an ESI-MS interface typically transmits ion beams continuously,<sup>51–56</sup> the ESI-IMS funnel must provide ions in discrete packets and, thus, has been designed to accumulate and store ions between the pulses for IMS introduction. Ions are stored between the funnel exit electrode and the following ion gate. In a typical ion funnel design having a 2-mm exit aperture, this is a volume of only a few cubic millimeters. A regular funnel has been previously used for interfacing ESI with IMS.<sup>57</sup> However, in that case, the IMS drift tube was of  $L = 4.5$  cm only, allowing a high IMS injection frequency (1–10 kHz). That is, the funnel had to accumulate or store ions for only 0.1–1 ms. The present high-resolution IMS is 210 cm long, and the funnel should ideally accumulate and store ions for as long as  $\sim 50$ –100 ms between IMS pulses. The total charge accumulated from an ion beam arriving over that time can be substantial and easily exceed the storage capacity of a volume of several cubic millimeters.

The present hourglass ion funnel design<sup>58</sup> greatly increases the ion storage volume while maintaining the differential pumping required between the ESI source chamber and IMS tube. Similar to our conventional ion funnel,<sup>56</sup> this device consists of 100 ring electrodes (machined from 0.5-mm-thick brass) separated by 0.5-mm-thick Teflon sheet spacers. These are divided into three sections: the front section of 24 electrodes with i.d. of 25.4 mm, the middle section of 42 electrodes with i.d. decreasing linearly from 25.4 to 2.0 mm, and the rear section of 34 electrodes with i.d. increasing linearly from 2.5 to 20.0 mm at the ion funnel exit to the IMS. The 2-mm aperture also serves as the conductance limit between the source chamber and the IMS drift tube. As in a normal funnel, rf and dc voltages are applied simultaneously to

each electrode.<sup>56</sup> The frequency and the (peak-to-peak) amplitude of rf are 500 kHz and 90 V, respectively. The dc biases of  $\sim 330$  V on the first and  $\sim 90$  V on the last funnel electrodes produce an axial dc field of  $\sim 24$  V/cm in the funnel, which provides efficient ion transmission to the IMS stage. To disperse the expansion jet from the heated capillary exit and improve the uniformity of gas flow in the funnel, a “jet disrupter” element was incorporated at the funnel axis 20 mm from the entrance.<sup>59,60</sup> This element consists of a metal disk (o.d. 6.5 mm) that is insulated from the rest of the funnel, allowing an independent voltage control. The typical jet disrupter voltage is  $\sim 308$  V.

About 2 mm after the last funnel electrode is an ion “gate” constructed of high-transmission grid (20 lines/in., Buckbee-Mears, St. Paul, MN). Normally, at 115 V, the gate confines ions to the end of the exit region of the ion funnel. To inject ions into IMS, the gate is pulsed open by a rectangular waveform that drops the grid to 42 V. The waveform is synthesized using an electrically floated generator, with the pulse frequency and duration controlled via a trigger signal sent through an optical cable. In this work, we used pulses of 50- $\mu$ s duration. Between pulses, ions are accumulated in the region between the last funnel electrode and the ion gate that has a volume of  $\sim 600$  mm<sup>3</sup>,  $\sim 2$  orders of magnitude greater than that in the conventional funnel configuration.

The floating voltage is provided by a 60-kV dc power supply (Glassman, High Bridge, NJ) and monitored by a custom high-voltage probe with accuracy of  $<0.1\%$ . The line ac power is fed into the floated electronic control box through a high-voltage transformer (Del Electronics, Valhalla, NY) that raises the ac output to IMS voltage.

**IMS Drift Tube.** The drift tube is a modular assembly of identical units, which offers a variable IMS length and other advantages. Each unit consists of a stack of 21 ring electrodes housed in a 20-cm-long cylindrical chamber (i.d. 20 cm, nonmagnetic steel) with vacuum flanges on both ends. Units are electrically insulated by 1-cm-thick PEEK disks (vacuum-sealed by O-rings) and assembled into a tube using insulating bolts and nuts (reinforced fiberglass). The disks feature center holes for ion

(57) Wyttenbach, T.; Kemper, P. R.; Bowers, M. T. *Int. J. Mass Spectrom.* **2001**, *212*, 13.

(58) Smith, R. D.; Tang, K.; Shvartsburg, A. A. U.S. Patent, 6,828,890, 2004.

(59) Kim, T.; Tang, K.; Udseth, H. R.; Smith, R. D. *Anal. Chem.* **2001**, *73*, 4162.

(60) Smith, R. D.; Kim, T.; Tang, K.; Udseth, H. R. U.S. Patent 6,583,408, 2003.

passage and blind holes on both sides for mounting four 21-cm-long solid ceramic rods (3.2 mm in diameter) that support the copper ring electrodes (i.d. 55 mm, o.d. 80 mm) inside each unit. These electrodes are uniformly spaced and mutually insulated by tubular plastic spacers of  $\sim 10$ -mm length. All electrodes in the tube are consecutively connected by high-precision 1-M $\Omega$  resistors. The median ring of each unit is electrically shorted to its chamber; i.e., the voltages on chambers decrease along the tube in equal steps. This minimizes the voltage difference between a ring and nearest chamber wall at any point along the tube, which reduces the risk of electrical gas breakdown inside IMS and thus maximizes the achievable drift voltage and the obtainable resolution. The present IMS includes up to 10 units with total  $L = 210$  cm. Further lengthening through additional units is straightforward. The dc floating voltage generated as described above is applied to the first electrode of front unit using a high-voltage feed-through on the chamber wall, while the voltage of the last electrode of back unit (normally 240 V) is set by a dc power supply referenced to ground. The resistor chain partitions the difference between those two voltages (the IMS drift voltage) across the drift tube. The front unit of IMS is interfaced to the ESI source chamber. For a smoother coupling, the first two IMS electrodes have a reduced i.d. (20 mm), the same as the aperture of the last ion funnel electrode.

The IMS-MS ion funnel operates conventionally as no ion storage step is needed. To capture all ions from the drift tube, this ion funnel has an acceptance diameter of 51 mm, only slightly smaller than the IMS electrode aperture and approximately twice that of the ESI-IMS hourglass ion funnel developed here or other ion funnels used previously for ESI-MS.<sup>51–57</sup> Over the 84-mm funnel length, the i.d. of the 84 electrodes decreases linearly to 2.5 mm. The funnel is powered by adjustable rf and dc power supplies referenced to ground. The rf is normally 500 kHz with an (peak-to-peak) amplitude between 0 and 80 V. Typical dc biases are  $\sim 200$  V on the first electrode and  $\sim 50$  V on the last, creating an axial gradient of  $\sim 18$  V/cm in the funnel. Matching this gradient to the IMS drift field may smooth the motion of ions entering the funnel. As in previous designs, following the last funnel electrode is a dc-only electrode at  $\sim 40$  V with a 2-mm-diameter orifice that serves as the IMS-MS conductance limit.

The drift tube is continuously filled with buffer gas through two gas distribution lines introduced near the IMS terminus. Any buffer gas or mixture of gases could be employed; presently we use dry N<sub>2</sub>. Needle valves installed on the distribution lines provide a fine control of gas inflow and, thus, of the IMS pressure  $P$ . Two capacitance manometers (MKS, Wilmington, MA) measure the pressures in the IMS and the source chamber with 0.1% accuracy over the 0–20-Torr range. Gas must flow from the drift tube into source chamber, to prevent gases from the ESI source (here atmospheric air) from diluting the IMS buffer gas. This counterflow is also critical to prohibit volatile neutrals from entering the IMS where they could become ionized via charge-transfer reactions or complex to analyte ions. Therefore, the drift tube is slightly overpressured relative to the ESI interface source chamber. This is achieved by adjusting  $P$ , source chamber pressure as described above, or both.

**TOF MS.** The MS analysis of ion packets separated in the IMS is performed by a modified commercial QTOF (Sciex Q-Star

Pulsar, Concord, Canada) with MS resolving power of 6000–10 000. At typical IMS operating pressure ( $P > 1$  Torr), the gas outflow through the 2-mm orifice at the IMS-MS interface would significantly raise the pressure in the collisional cooling quadrupole chamber of MS (Q0 in Figure 1). This would result in long ion transit times through that region that would unacceptably distort the IMS measurements and degrade the resolution. This issue was addressed by adding a stage of differential pumping after IMS. This has been engineered as a small chamber containing a 24-mm-long quadrupole (Q00 in Figure 1) set to pass all ions (rf only at 912 kHz and 200 V peak to peak). Following Q00 is a lens with 2.5-mm aperture that provides the conductance limit to MS. The dc voltages on quadrupole rods and the lens are adjustable and typically set at 35 and 25 V, respectively. The chamber is evacuated by a mechanical pump (Alcatel 2033, 12.8 L/s). This lowers the pressure in Q00 by 1 order of magnitude compared to that in IMS (e.g.,  $\sim 0.3$  Torr vs  $P = 4$  Torr), and the gas outflow to Q0 is reduced proportionately. No significant dissociation of ions in Q00 has been observed under these conditions.

The TOF MS has a four-channel ion detector system. Ion counts from each channel stream into a related time-to-digital converter (TDC). The Q-Star TDC was upgraded to 10-GHz TDC (Ortec 9353, Oak Ridge, TN), currently the fastest commercial TDC. This, however, is a single-channel TDC, so the ion counts from all four detector channels were initially combined after the preamplifier (Figure 2a). The timing sequences of IMS pulsing and MS data acquisition are set by an I/O control board (National Instruments PCI-6711). Both TDC and that board are installed in a PC (Dell with the Windows XP operating system). The overall instrument control software runs on the same PC.

**Control Software.** The Q-Star data acquisition software (Sciex Analyst) does not store individual TOF spectra, but averages them over a preset period of time. This would obviously lose all information from IMS separation. The software also has no capability to control IMS operation and coordinate it with MS analyses. Hence we developed a new software to provide the overall instrument control, storage, and processing of the 2-D IMS-MS data. However, TOF is still operated by the Sciex Analyst resident on its original instrument PC. In particular, Analyst sets the TOF pusher period (normally in the 100–140- $\mu$ s range) depending on the upper  $m/z$  limit desired. To synchronize IMS and MS operations, the IMS pulsing period is divisible by the pusher period (e.g., 500 TOF spectra lasting 100  $\mu$ s each are acquired during 50 ms between IMS pulses). Beyond that constraint, the period and duration of IMS pulse are user-defined.

The software was designed in Visual Basic 6 and implemented on top of the ActiveX controls running the Ortec hardware. The system collects and stores a user-defined number of sequential 2-D maps, each derived by averaging a certain number of elementary IMS-MS frames. The acquisition of first frame starts from a random TOF pusher pulse (Figure 2b). Triggered by that pulse, a call is issued to open the IMS ion gate (as described above) and simultaneously start the data acquisition process. The software then maps the ion counts recorded by the TDC onto a 2-D frame, filling a sequence of “0” and “1” in each segment of IMS drift time equal to the TOF pusher period. This continues

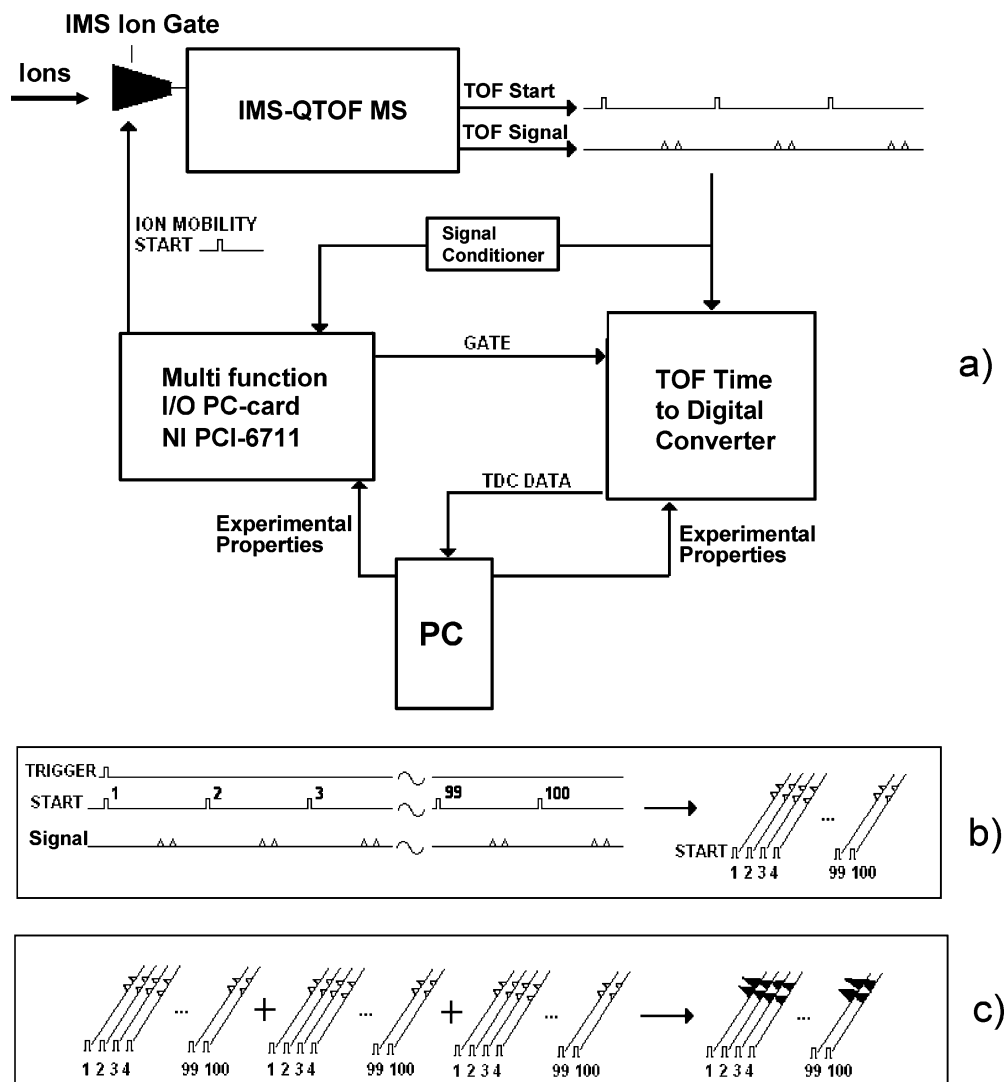


**Figure 2.** Diagram of the instrument control and data acquisition system (a) and sequence of events during IMS-MS data collection (b, c).

for a preset integer number of periods up to the desired maximum IMS drift time (Figure 2b). In the end, each frame pixel contains a “1” if an ion has arrived within corresponding bins of drift time and TOF flight time, and a “0” otherwise. The program then resets the experiment and starts acquiring the next frame coincidentally with a TOF pusher pulse. All following frames up to a predefined number (typically 100–1000) are given as a histogram on top of the first (Figure 2c). This process transforms a binary series in each IMS drift time segment into a TOF spectrum. This spectrum is converted into a mass spectrum using calibration and standard formulas relating  $m/z$  of ions to their flight times. A typical 2-D map generated is shown in Figure 3a. A mass spectrum of the same sample acquired using the TOF MS data system (Figure 3b) is clearly identical to the projection of 2-D map in Figure 3a on the  $m/z$  axis.

For tuning and evaluation of ion transmission efficiency, the instrument may be operated in a continuous mode. In that regime, the IMS ion gate is permanently open and TOF spectra are acquired by Analyst as usual. Peptides and other chemicals used in the instrumental evaluation are available from Sigma Aldrich.

## RESULTS AND DISCUSSION

In the low-field regime, ion mobilities are independent of the drift field. The ion mobility is derived<sup>21</sup> from IMS measurements as

$$K = L^2 / (Ut_D) \quad (5)$$

where  $U = EL$  is the drift voltage. Hence  $t_D$  is proportional to  $1/U$  for any IMS length and gas pressure. However, in IMS-MS, one measures not  $t_D$ , but the arrival time  $t_A$ —the sum of times spent by an ion in all parts of the instrument between injection into IMS and detection. Previously, this was given by  $t_A = \{t_D + t_{MS}\}$ , where  $t_{MS}$  was the time in MS analyzer (e.g., QTOF) following IMS.<sup>36</sup> This is now modified to  $t_A = \{t_D + t_{IF} + t_{MS}\}$ , where  $t_{IF}$  is the transit time through the IMS-MS ion funnel. The values of  $t_{IF}$  and  $t_{MS}$  are determined by conditions in, respectively, the funnel and QTOF and are almost independent of IMS parameters such as  $U$  or  $L$ . Thus,  $t_A \propto 1/U$  will be true only when  $t_A \approx t_D$ ; i.e., when  $\{t_{IF} + t_{MS}\} \ll t_D$ . The presently measured  $t_A$  times are indeed linear versus  $1/U$  at different  $P$ , even for a shorter drift tube ( $L = 105$  cm) and a proportionately smaller  $t_D$  (Figure

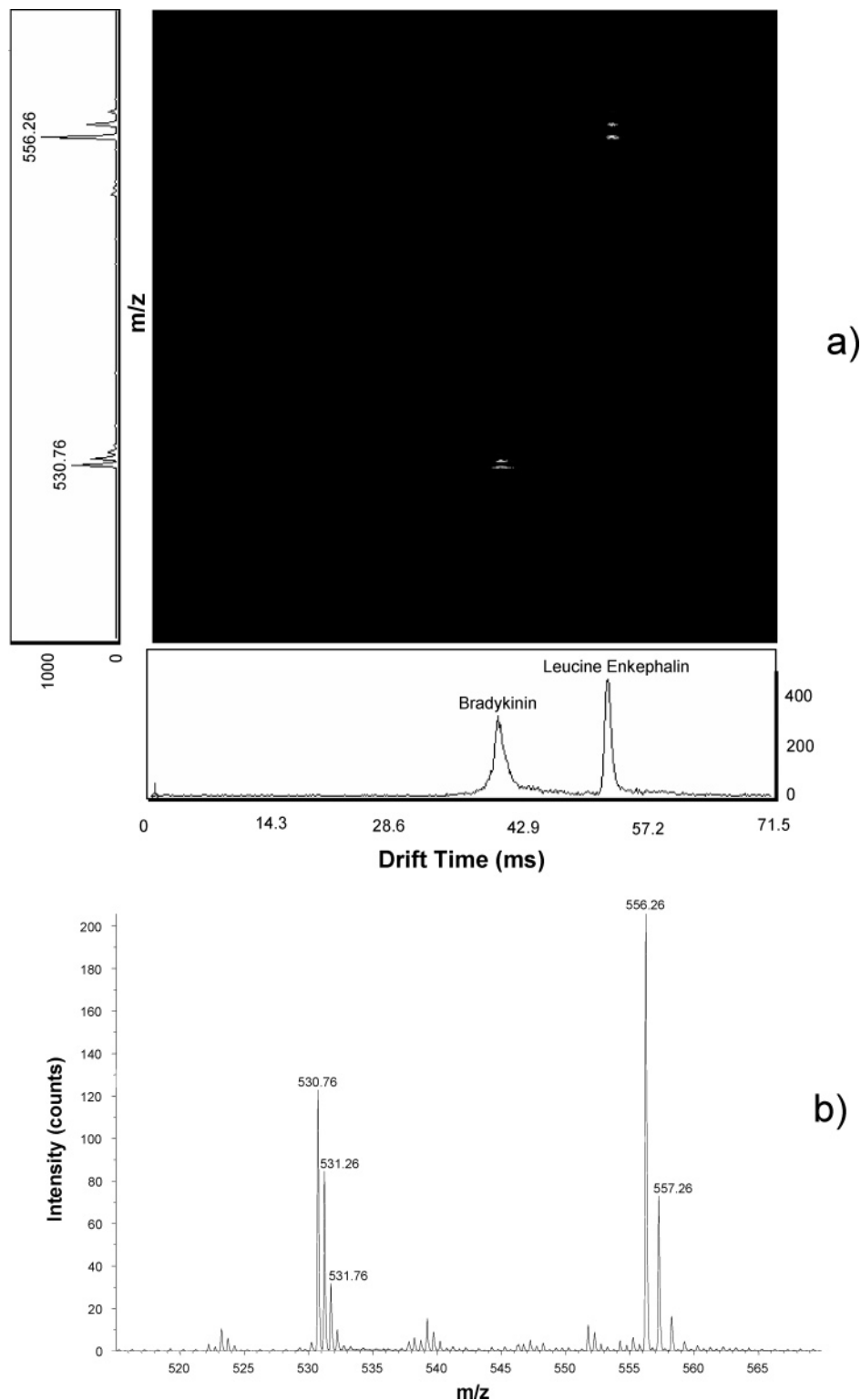


**Figure 3.** Demonstration of the data processing approach: (a) a 2-D map with projections on the drift time (horizontal) and  $m/z$  (vertical) axes; (b) the mass spectrum obtained by Sciex Analyst for the same sample—a 1:1 mixture of Le-Enk (5  $\mu\text{M}/\mu\text{L}$ ) and bradykinin. IMS parameters:  $L = 210$  cm,  $U = 4.76$  kV, and  $P = 4.02$  Torr.

4). Hence, an ion funnel at the IMS end does not delay ions significantly and therefore does not degrade the resolution of IMS analyses.

**Lossless IMS-MS Separations.** As described above, ion funnels have been incorporated into our ESI-IMS-QTOF design to provide more efficient ion transmission. Essentially perfect ion transmission has been achieved from the IMS to the TOF. The

performance was evaluated using protonated peptide ions that cover the range of masses ( $m \sim 0.5\text{--}6$  kDa) and charge states ( $z = 1\text{--}5$ ) typical for bottom-up proteomics: leucine enkephalin ( $m = 556$  Da,  $z = 1$ ) – below Le-Enk, bradykinin ( $m = 1061$  Da,  $z = 2$ ), Glu-fibrinopeptide B ( $m = 1572$  Da,  $z = 2$ ), and insulin ( $m = 5735$  Da,  $z = 5$ ). In the first test, ion signals obtained for continuous operation (i.e., without IMS pulsing) were bench-

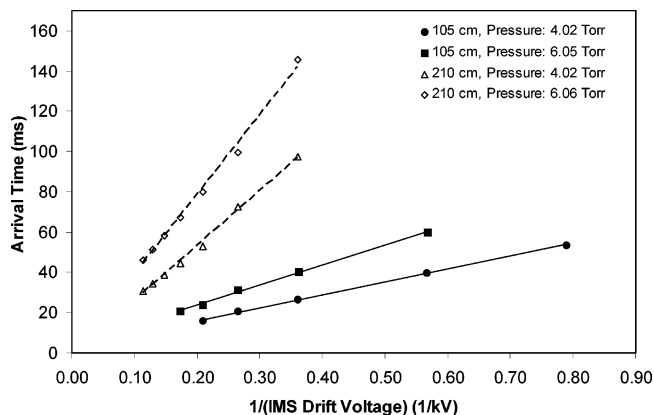


**Figure 4.** Independence of measured mobility of the IMS drift voltage under various instrumental conditions. Arrival times of Le-Enk as a function of drift voltage at two gas pressures and two drift tube lengths are as marked (10 pM/ $\mu$ L sample infused at 0.5  $\mu$ L/min).

marked versus those measured on a usual ESI-QTOF with no drift tube. To ensure a proper comparison, the standard OSC interface of QTOF was replaced by an *exact copy* of the present capillary–ion funnel interface with IMS-QTOF. The intensities of mass spectra acquired on those two instruments for same samples and ESI conditions (Figure 5 a,b) differ by less than a factor of 2, a customarily accepted uncertainty of such comparisons. Therefore, the cumulative ion transmission efficiency through a 147-cm-long IMS stage and IMS-MS interface exceeds 50% and likely approaches 100%. In another test, we measured ion intensities in ESI-IMS-QTOF as a function of drift tube length. Combining eqs 1 and 3, one may derive (when  $\Theta \ll L/R$ )

$$S \sim \frac{\Theta^2 Eze}{16k_B TL \ln 2} \quad (6)$$

That is, when the ion beam inside the IMS diverges significantly beyond the reach of exit funnel, the signal scales as  $\sim 1/L$ . This is not observed experimentally: for example, sensitivities at  $L = 105$  cm and  $L = 210$  cm are equal within estimated uncertainty (Figure 5c). The fact that doubling the IMS length does not measurably affect the ion intensity further proves an essentially lossless ion transmission through the IMS and to the TOF.

To realize high ion transmission efficiencies, ions exiting the IMS must obviously enter the mouth of the IMS-MS ion funnel. When an ion packet width exceeds the funnel entrance aperture, the signal should decrease according to eqs 1–3. To confirm this, we probe ion intensities as a function of  $E$  (i.e., the drift voltage) present in eq 3. For example at  $U = 3.8$  kV, eqs 2 and 3 yield  $R_d \approx 110$  and for the spatial width of initial ion packet equal to 20 mm (the exit aperture of hourglass funnel from which ions enter IMS),  $R \approx 75$ . The fwhm of ion beam at IMS end (for  $L = 210$  cm) would be  $\sim 28$  mm. Assuming a Gaussian density distribution across the ion beam ( $>95\%$  of which is found within 2 fwhm), the “outside” diameter of ion beam approaching the exit funnel is  $\sim 43$  mm. That would bring the beam circumference within 4 mm of the funnel entrance ring (i.d. 51 mm). So, when  $U$  is decreased, the sensitivity should remain constant until  $U \sim 3.5$ –4 kV and then start dropping. Experiments verify this prediction quantita-

tively (Figure 6). These results indicate that ion losses through an IMS of any length can be eliminated completely as long as the IMS electrodes and ion funnel entrance are slightly larger than the ion packet width.

The high sensitivity of the present instrument provided by near-perfect ion transmission through IMS allows fast IMS-MS data acquisition. For example, a well-defined peak ( $S/N = 6$ ) is obtained in just 0.6 s by averaging 10 elementary frames (Figure 7a). The high stability of the present system is evident from a linear dependence of the cumulative ion signal on acquisition time (Figure 7b). The present sensitivity performance can be further improved (possibly several orders of magnitude) by operating electrospray in the nanoelectrospray regime.<sup>61,62</sup>

#### No Effect of the Terminal Ion Funnel on IMS Resolution.

The key question already mentioned is whether the rf fields in the IMS-MS ion funnel (or its refocusing of ions from the IMS terminus) degrade IMS separation performance measured by the MS stage. The present measurements show convincingly that any degradation is insignificant; neither the drift time nor resolution exhibits any dependence on the rf amplitude, extending to zero V where the funnel operates in a dc-only mode that provides no ion focusing (Figure 8). Of course, the sensitivity drops by nearly 2 orders of magnitude as the rf voltage decreases (Figure 8), and the attenuation curve closely tracks that observed for an ion funnel at the API-MS interface.<sup>54</sup> This directly demonstrates that the present virtually lossless ion transmission through IMS is achieved by rf ion focusing in electrodynamic funnels.

To gain a deeper insight into the temporal aspects of ion focusing at the IMS terminus, we have modeled the passage of realistic ion packets approaching from IMS through the IMS-MS funnel. These classical molecular dynamics simulations follow a statistically representative ion ensemble evolving under the influence of external (rf and dc) fields, thermal diffusion, and mutual Coulomb repulsion of constituent ions. This approach was successful in modeling and optimizing funnels for continuous ion transmission,<sup>52,56,63</sup> where the kinetics of ion motion is not an issue. Here we use the same procedure to track the movements of discrete ion packets in time. The principal conclusion is that, under experimental conditions of this work, the  $t_{IF}$  time for any ion depends almost exclusively on its mobility and the axial dc field; i.e., a funnel effectively becomes another IMS stage. In agreement with experiment, the rf fields in this regime have but a negligible effect on  $t_{IF}$  and thus on IMS resolution. This is not always the case: increasing the rf amplitude, decreasing the frequency excessively, or both eventually creates a ladder of potential energy wells along the funnel axis that deepen toward the exit.<sup>63</sup> This effectively turns the funnel into a sequence of ion traps. Such operation would lengthen  $t_A$  and degrade the resolution by remixing ions separated in IMS, as well as reduce the ion transmission efficiency of the funnel. Thus, the sensitivity and IMS resolution of IMS-MS are maximized over essentially the same operating conditions. In other words, no reason exists to operate the funnel in a mode that would degrade IMS performance.

(61) Schmit, A.; Karas, M.; Dulcks, T. *J. Am. Soc. Mass Spectrom.* **2003**, *14*, 492.

(62) Tang, K.; Page, J. S.; Smith, R. D. *J. Am. Soc. Mass Spectrom.* **2004**, *15*, 1416.

(63) Tolmachev, A. V.; Kim, T.; Udseth, H. R.; Smith, R. D.; Bailey, T. H.; Futrell, J. H. *Int. J. Mass Spectrom.* **2000**, *203*, 31.

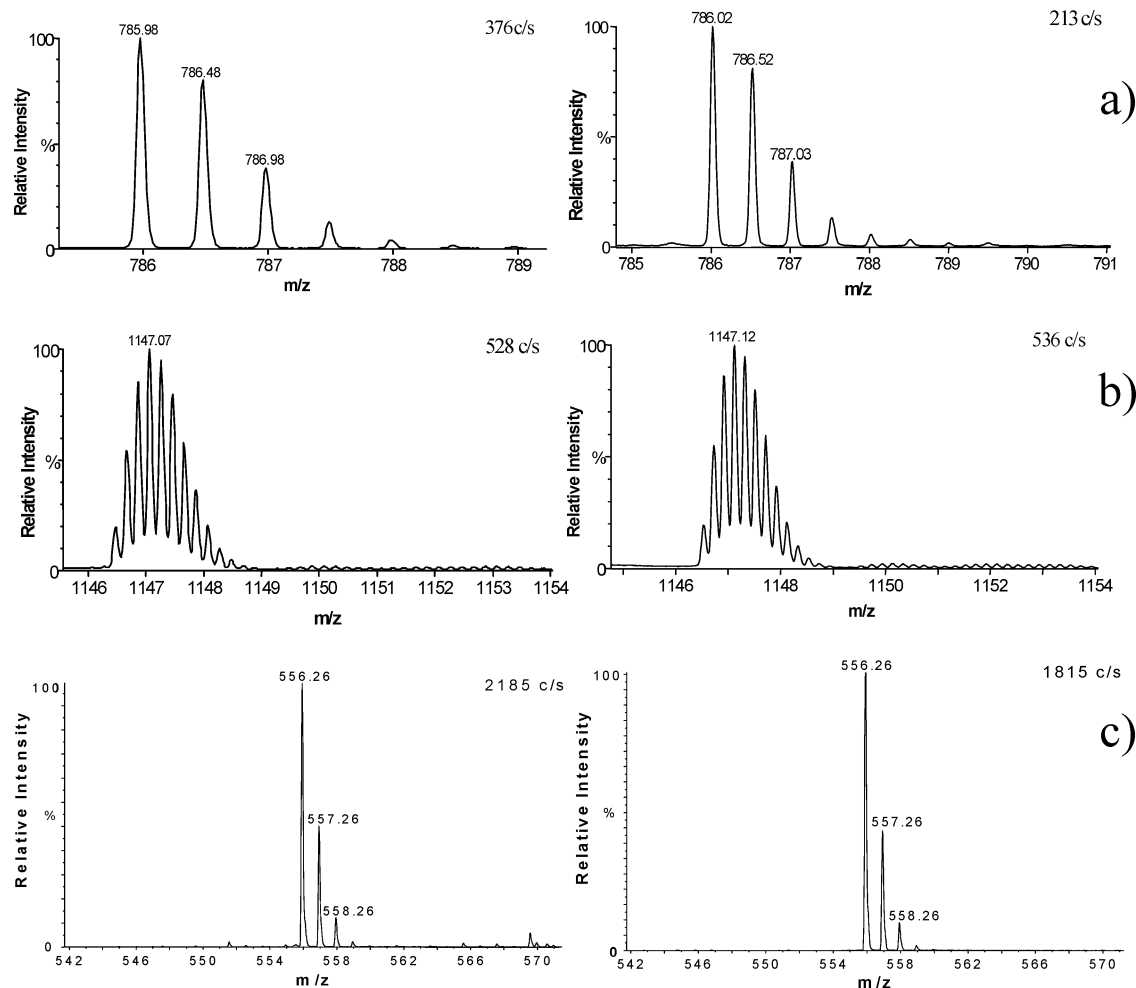


**Figure 5.** Benchmarks for different instrumental configurations proving lossless IMS transmission. In (a) and (b) are the mass spectra for (a)  $(\text{H}^+)_2$ Glu-fibrinopeptide B (0.1  $\text{pM}/\mu\text{L}$ ) and (b)  $(\text{H}^+)_5$ insulin (0.2  $\text{pM}/\mu\text{L}$ ) obtained using capillary–ion funnel interfaced with QTOF (left) and IMS-QTOF at  $L = 147$  cm (right). In (c) are the mass spectra for Le-Enk (10  $\text{pM}/\mu\text{L}$ ) obtained using ESI-IMS-QTOF at  $L = 105$  cm (left) and  $L = 210$  cm (right). The IMS was operated at  $U = 2.76$  kV and  $P = 2$  Torr (a, b),  $U = 1.76$  kV and  $P = 4$  Torr (c, left), and  $U = 5.76$  kV and  $P = 4$  Torr (c, right).

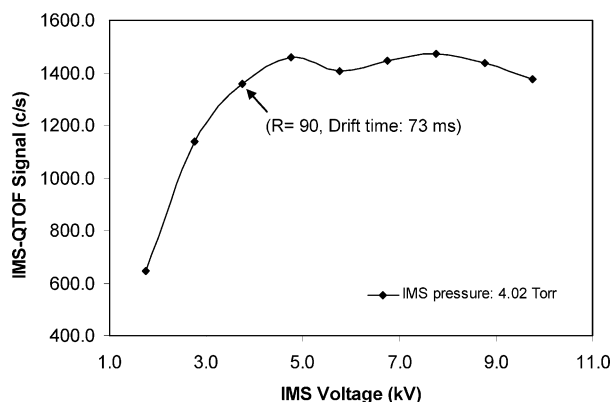


**Figure 6.** IMS-QTOF sensitivity versus IMS drift voltage (for Le-Enk, 10  $\text{pM}/\mu\text{L}$  solution,  $L = 210$  cm).

In calculations, the IMS-MS funnel also “chokes” at very high currents that exceed its charge capacity in the narrowest region near the exit.<sup>64</sup> This is, however, unlikely in reality as long

as the conductance limit of the ESI-IMS funnel does not significantly exceed that of the IMS-MS funnel. Thus, the performance of the funnel as an ion collector at the IMS-MS interface should not be compromised by obtainable peak intensities.

The currently achieved IMS resolving power of 90–120 for singly charged ions (Figures 7a and 8) is slightly short of the best reported performance<sup>35,36</sup> ( $R = 150$ – $170$ ). However, this is only because of a lower drift voltage: 4.76 kV at present versus 10–14 kV in previous studies.<sup>35,36</sup> Higher voltages could potentially cause electrical discharges in rarefied buffer gases. (Gases are most prone to electrical breakdown at pressures of a few Torr where the minimums of Paschen curves are typically found.<sup>65</sup>) All high-resolution IMS spectra in the literature have been obtained at much higher  $P$  (>200 Torr) that allow stronger electric fields. As we discussed, those instruments have lower sensitivity when coupled to MS. Also, lower-pressure drift tubes are suitable for MS-IMS-MS systems with mass selection both before and after IMS separation,<sup>2,3</sup> a critical capability for many applications.<sup>66</sup> High-pressure IMS is incompatible with such designs since polyatomic

(64) Shvartsburg, A. A.; Tang, K.; Tolmachev, A. V.; Anderson, G. A.; Smith, R. D. *Proceedings of the 52nd ASMS Meeting*, Nashville, TN, 2004.

(65) *Electrical Breakdown of Gases*; Meek, J. M.; Craggs, J. D., Eds.; Wiley: New York, 1978.

(66) Shvartsburg, A. A.; Jarrold, M. F. *Phys. Rev. Lett.* **2000**, *85*, 2530.

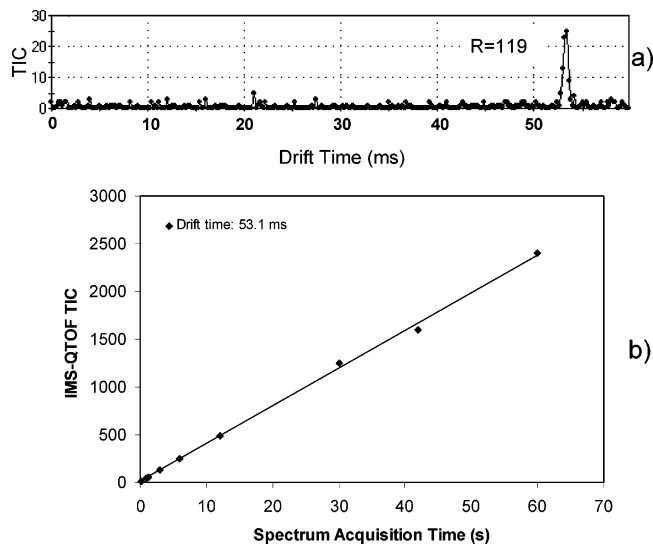


**Figure 7.** High instrumental sensitivity and stability: (a) IMS drift time distribution acquired in 0.6 s; (b) cumulative IMS-QTOF signal as a function of acquisition window (for Le-Enk, 10 pM/ $\mu$ L solution,  $L = 210$  cm,  $U = 4.76$  kV,  $P = 4.02$  Torr).

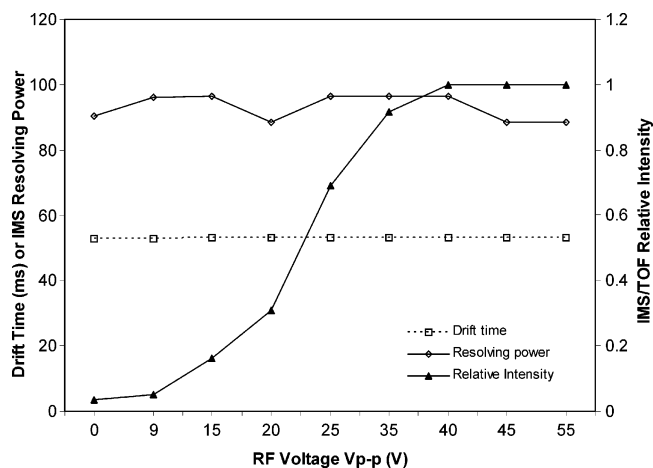


**Figure 8.** Effect of the rf amplitude on the IMS-MS funnel on IMS drift time, resolution, and sensitivity (conditions as in Figure 7).

ions cannot be effectively injected in the high pressure differential of the MS-IMS junction: the electric field is either insufficient to pull ions against a gas flow out of IMS or high enough to fragment them through collisional heating.

The key metric of IMS design quality is the measured resolving power as a fraction of theoretical limit.<sup>45</sup> At the conditions of Figures 7 and 8,  $R_d = 129$  by eq 3 and more precisely  $R_d = 127$  correcting for the high-field anisotropic diffusion.<sup>44</sup> Taking into account finite widths<sup>45</sup> of the ion injection pulse (50  $\mu$ s) and TOF acquisition window (100  $\mu$ s) reduces  $R$  to 120, and the measured  $R$  of  $\sim 90$ –119 is  $\sim 75$ –99% of that value. As a benchmark, the highest performance drift tubes with flat end plates exhibit 80–88% of the theoretical limit in stand-alone IMS,<sup>45</sup>  $\sim 90\%$  in IMS-quadrupole MS,<sup>36</sup> and  $\sim 70$ –100% in IMS-TOF.<sup>32</sup> This again demonstrates that an ion funnel at the IMS-MS interface does not degrade IMS resolution.

## CONCLUSIONS

We have developed new ESI-IMS-TOF instrumentation for rapid, sensitive analyses of complex mixtures based on ion mobility separations followed by mass spectrometry. The instrumentation has two major attractions: an extremely high throughput of gas-phase separation and the simultaneous dispersion of all ions in IMS and MS dimensions. The key distinction of the present instrument is the usage of electrodynamic ion funnels at both the ESI-IMS and IMS-TOF MS interfaces. Other innovations include (a) an hourglass ion funnel for effective ion transmission in the pulsed mode (employed here to accumulate ions arriving from the source and inject them into IMS), (b) a modular IMS design that provides experimental flexibility, permits a record drift tube length (here 210 cm), and minimizes the electrical breakdown hazard, and (c) the new wide ion funnel with acceptance aperture over 5 cm (double that of the largest earlier designs).

A near-perfect ion collection by the IMS terminal ion funnel results in virtually lossless ( $>50\%$ ) transmission of ions across a broad  $m/z$  range relevant to most biological analyses, through an IMS of any length, and to the TOF MS stage. The ion drift time (mobility) and IMS resolution are not degraded by ion funnel operation. In particular, the measured IMS resolving power exceeds 100 and amounts to  $>80\%$  of the theoretical limit, which is comparable to the best reported IMS or IMS-MS performance. The sensitivity of the ESI-IMS-QTOF was close to that of the unmodified ESI-MS; i.e., the IMS separation capability is added “for free” in terms of either sensitivity or throughput. This development allows one to handle a greater sample complexity within the same time, increase the throughput without sacrificing quality, or both, which should make IMS-MS an attractive practical platform for biological analyses and other demanding high-throughput applications. Further increases in overall separation power can be obtained by the combination with prior fast condensed-phase separations (e.g., using capillary electrophoresis or LC) or another gas-phase separation stage based upon differential IMS (FAIMS), as will be described elsewhere. Finally, further increases in sensitivity are anticipated from optimization of the ion accumulation process in the first ion funnel and ESI operation using low nanoliter per minute flow rates where ionization efficiencies can approach 100%.<sup>61,67</sup>

## ACKNOWLEDGMENT

The authors thank the Laboratory Directed Research and Development Program and the NIH National Center for Research Resources (RR18522) for supporting portions of this research. We also thank Professor David Clemmer (Indiana University) for helpful discussions. Pacific Northwest National Laboratory is operated by the Battelle Memorial Institute for the U.S. Department of Energy through Contract DE-AC05-76RLO1830.

Received for review November 15, 2004. Accepted March 15, 2005.

AC048315A

(67) Smith, R. D.; Shen, Y.; Tang, K. *Acc. Chem. Res.* **2004**, *37*, 269.